Journal of Solid State Chemistry 182 (2009) 295–300

Contents lists available at ScienceDirect

Journal of Solid State Chemistry

journal homepage: www.elsevier.com/locate/jssc

Crystal growth of a series of lithium garnets $Ln_3Li_5Ta_2O_{12}$ (Ln = La, Pr, Nd): Structural properties, Alexandrite effect and unusual ionic conductivity

Irina P. Roof [a], Mark D. Smith [a], Edmund J. Cussen [b], Hans-Conrad zur Loye [a,*]

[a] Department of Chemistry and Biochemistry, University of South Carolina, Columbia, SC 29208, USA
[b] WestCHEM, Department of Pure and Applied Chemistry, Thomas Graham Building, The University of Strathclyde, 295 Cathedral Street, Glasgow G1 1XL, UK

ARTICLE INFO

Article history:
Received 20 August 2008
Received in revised form
21 October 2008
Accepted 25 October 2008
Available online 8 November 2008

Keywords:
Hydroxide flux
Crystal growth
Tantalates
Lanthanides
Alexandrite effect
Lithium ionic conductivity
Optical properties

ABSTRACT

We report the single crystal structures of a series of lanthanide containing tantalates, $Ln_3Li_5Ta_2O_{12}$ (Ln = La, Pr, Nd) that were obtained out of a reactive lithium hydroxide flux. The structures of $Ln_3Li_5Ta_2O_{12}$ were determined by single crystal X-ray diffraction, where the Li^+ positions and Li^+ site occupancies were fixed based on previously reported neutron diffraction data for isostructural compounds. All three oxides crystallize in the cubic space group $Ia\bar{3}d$ (No. 230) with lattice parameters a = 12.7735(1), 12.6527(1), and 12.5967(1) Å for $La_3Li_5Ta_2O_{12}$, $Pr_3Li_5Ta_2O_{12}$, and $Nd_3Li_5Ta_2O_{12}$, respectively. A UV–Vis diffuse reflectance spectrum of $Nd_3Li_5Ta_2O_{12}$ was collected to explain its unusual Alexandrite-like optical behavior. To evaluate the transport properties of $Nd_3Li_5Ta_2O_{12}$, the impedance data were collected in air in the temperature range $300 \leqslant T(^\circ C) \leqslant 500$.

1. Introduction

As part of our ongoing work on the crystal growth of new oxides using molten alkali metal hydroxides fluxes, [1–6] we were able to obtain single crystals of the title compounds $Ln_3Li_5Ta_2O_{12}$ (Ln = La, Pr, Nd). Hydroxide fluxes are an excellent medium for the dissolution of lanthanide oxides, late transition metals, such as iridium [2,4], ruthenium [1,3] and, as recently demonstrated, early transition metal oxides, such as niobium and tantalum oxide [5–7]. In our investigation to prepare mixed lanthanide/early transition metal oxides, we obtained single crystals of a series of lanthanum containing tantalates with nominal formula $Ln_3Li_5Ta_2O_{12}$ (Ln = La, Pr, Nd). While the existence of $La_3Li_5Ta_2O_{12}$ had been determined during the exploration of the La_2O_3–Ta_2O_5–Li_2O phase space [8] and subsequently been prepared as a polycrystalline powder [9], the other two members, $Pr_3Li_5Ta_2O_{12}$ and $Nd_3Li_5Ta_2O_{12}$, represent new composition and their syntheses, optical properties, and structures are reported for the first time herein.

Complex lanthanide containing oxides comprise an interesting group of materials that exhibit many intriguing properties including fast lithium ion conduction [9–15] and unusual optical properties [16–19]. The continued interest in fast lithium ion conductors for use in rechargeable lithium ion batteries [12,14,15,20–23] has recently led to the investigation of materials with garnet related structures, such as, $Li_5La_3Bi_2O_{12}$ and $Li_6SrLa_2Bi_2O_{12}$ [11], $Li_{3+x}Nd_3Te_{2-x}Sb_xO_{12}$ [24], $Li_{6.4}Sr_{1.4}La_{1.6}M_2O_{12}$ (M = Sb, Ta) [20] and $Li_7La_3Zr_2O_{12}$ [12], several of which have extremely high lithium ion conductivity. The title compounds, $Ln_3Li_5Ta_2O_{12}$ (Ln = La, Pr, Nd), also crystallize in the garnet structure and are, thus, of potential interest for their lithium ion conductivity. $Nd_3Li_5Ta_2O_{12}$, however, exhibits unusually low ionic conductivity. Results of our investigation are reported in this paper.

Lanthanide containing metal oxides are known to exhibit useful optical properties, such as room temperature photoluminescence [6] and laser light generation [16,17,19,25], and in some cases the optical properties are the direct result of the presence of a rare earth cation in the structure, for example neodymium, which causes some metal oxides to change color under different lighting conditions. Such a color changing phenomenon is known for some naturally occurring minerals, for example in Alexandrite, a Cr^{3+} doped chrysoberyl [26], as well as for lanthanide containing Monazite [27]. This rare dichroism is often referred to as the "Alexandrite Effect", for the mineral Alexandrite, which changes color depending on the source of the light (sun-light, incandescent light, fluorescent light) used to irradiate the mineral. The title compound, $Nd_3Li_5Ta_2O_{12}$, exhibits a type of Alexandrite effect that is described herein.

* Corresponding author. Fax: +1 803 777 8508.
E-mail address: zurloye@mail.chem.sc.edu (H.-C. zur Loye).

0022-4596/$ - see front matter © 2008 Elsevier Inc. All rights reserved.
doi:10.1016/j.jssc.2008.10.032

2. Experimental

2.1. Crystal growth

For the title compounds, 1 mmol of Ta_2O_5 (Acros Organics), 1 mmol of Ln_2O_3 (Alfa Aesar, 99.9%) and 4 g of LiOH•xH_2O (Alfa Aesar, 98%) were loaded into a silver tube that was previously flame sealed at one end. Lanthanide sesquioxides (La_2O_3 and Nd_2O_3) were activated prior to use in the synthesis by heating the oxides to 1000 °C for 24 h. Pr_2O_3 was prepared by heating Pr_6O_{11} at 1000 °C in flowing 5%/95% H_2/N_2 gas for 24 h with intermediate grinding using a programmable flow through tube furnace. Purity of all starting materials was verified by powder X-ray diffraction. Once loaded, the tubes were crimped shut and folded over three times before being placed upright into a programmable furnace. For all three compounds, the charges were heated to 600 °C in 1 h and held at the target temperature for 24 h. Subsequently, the charges were cooled by shutting off the furnace. The LiOH flux was dissolved in water aided by the process of sonication. Colorless, yellow and blue single crystals of $La_3Li_5Ta_2O_{12}$, $Pr_3Li_5Ta_2O_{12}$ and $Nd_3Li_5Ta_2O_{12}$, respectively, were isolated by vacuum filtration.

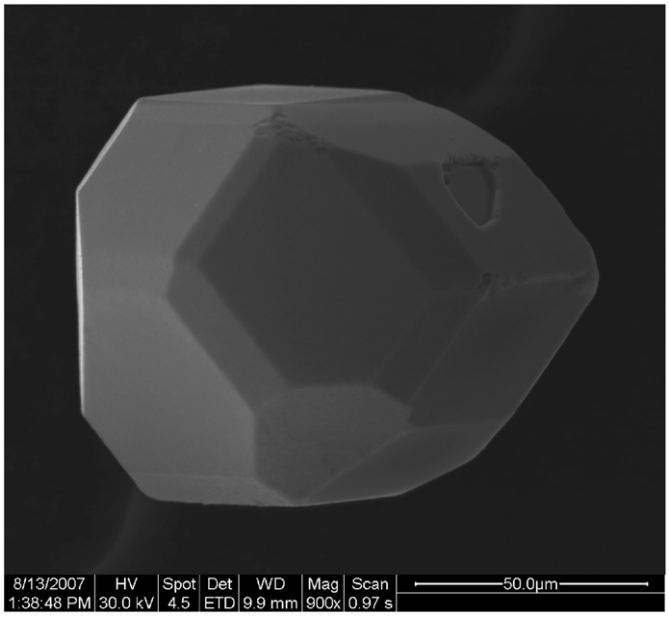

Fig. 1. SEM image of a typical $Nd_3Li_5Ta_2O_{12}$ single crystal, representative of the series $Ln_3Li_5Ta_2O_{12}$, grown out of a reactive lithium hydroxide flux.

2.2. Scanning electron microscopy

Environmental scanning electron micrographs of single crystals of $Ln_3Li_5Ta_2O_{12}$ (Ln = La, Pr, Nd) were obtained using a FEI Quanta 200 ESEM instrument. A scanning electron micrograph of a typical single crystal is shown in Fig. 1. Energy Dispersive Spectroscopy (EDS) verified the presence of tantalum and the respective lanthanide element, and, within the detection limits of the instrument, confirmed the absence of extraneous elements, such as silver.

2.3. Single crystal X-ray diffraction

Single crystal X-ray diffraction intensity data from multi-faceted colorless ($La_3Li_5Ta_2O_{12}$), yellow ($Pr_3Li_5Ta_2O_{12}$) or blue ($Nd_3Li_5Ta_2O_{12}$) prisms were measured at 150(1) K on a Bruker SMART APEX diffractometer (Mo$K\alpha$ radiation, $\lambda = 0.71073$ Å) [28]. The data collections covered a minimum of 99.7% of reciprocal space to $2\theta_{max} = 90^\circ$, with $R_{int} = 0.041$, 0.046, 0.039, and average redundancies of 29.4, 26.0, 29.1 for Ln = La, Pr, Nd, respectively. The raw area detector data frames were processed with SAINT+ [28], which also corrected for Lorentz and polarization effects. An absorption correction based on equivalent reflections was applied to the data with SADABS [28]. Difference Fourier calculations and full-matrix least-squares refinement against F^2 were performed with SHELXTL [29].

$La_3Li_5Ta_2O_{12}$ has been previously prepared by the traditional solid state method [22,30]. The Nd and Pr analogs have not previously been prepared and are isostructural with the lithium garnet $Li_5La_3Ta_2O_{12}$. There are three non-lithium atomic positions in this structure: Ln_1 (Wyckoff symbol 24c), Ta_1 (16a), and O_1 (96 h). Refinement of this structural model in the cubic space group $Ia\bar{3}d$ (No. 230) converged rapidly to R-values ($R1(F)$) of about 3% using only Ln, Ta, and O (i.e. no Li). At this stage there were two peaks in the difference map for each structure, corresponding to reasonable average positions for lithium atoms. The peaks had magnitudes near 3 and 2 $e^-/Å^3$ in each difference map, and were located near the centers of tetrahedral (Td, 24d, Li_1) and octahedral (Oh, 48 g, Li_2) sites, respectively. Refining these peaks as fully occupied lithium atoms resulted in unreasonable

Table 1
Crystal data and structural refinement for $La_3Li_5Ta_2O_{12}$, $Pr_3Li_5Ta_2O_{12}$ and $Nd_3Li_5Ta_2O_{12}$.

Empirical formula	$La_3Li_5Ta_2O_{12}$	$Pr_3Li_5Ta_2O_{12}$	$Nd_3Li_5Ta_2O_{12}$
Formula weight (g mol^{-1})	1005.33	1011.33	1021.32
Space group	$Ia\bar{3}d$	$Ia\bar{3}d$	$Ia\bar{3}d$
Unit cell dimensions			
a (Å)	12.7735(1)	12.6527(1)	12.5967(1)
V (Å^3)	2084.15(3)	2025.58(3)	1998.80(3)
Z	8	8	8
Density calculated (g cm^{-3})	6.408	6.633	6.788
Absorption coefficient (mm^{-1})	33.012	35.743	37.183
F (000)	3424	3472	3496
Crystal size (mm)	0.08 × 0.06 × 0.06	0.08 × 0.08 × 0.06	0.08 × 0.06 × 0.05
θ range	3.91–45.00	3.94–45.01	3.96–44.99
Reflections collected	22706	19627	21779
Independent reflections	722 ($R_{int} = 0.047$)	706 ($R_{int} = 0.0462$)	696 ($R_{int} = 0.0390$)
Goodness-of-fit on F^2	1.408	1.318	1.348
R indices (all data)	$R_1 = 0.0446$ w$R_2 = 0.0749$	$R_1 = 0.0394$ w$R_2 = 0.0640$	$R_1 = 0.0347$ w$R_2 = 0.0636$
Largest difference map peak and hole (e^- A^{-3})	2.043 and −2.065	1.842 and −1.629	2.260 and −1.787

thermal parameters and an excess of positive charge. However, refinement of the Li site occupancies both showed a decrease from unity, more reasonable thermal parameters, and a stable refinement. This provides good evidence for partial occupancy of both Td and Oh sites by lithium, despite the inherent uncertainty in determining lithium parameters from X-ray data. Free refinement of the occupancies and U_{iso} values of both sites yielded Li_1, 0.56(11) and 0.016(8) Å^2 and Li2, 0.23(7) and 0.015(8) Å^2, respectively, for Ln = La. These lithium parameters in the Ln = Pr and Nd crystals refined similarly. This corresponds to roughly three Li^+ per formula unit, or a charge excess of −2 per formula unit. Due to the fixed oxidation states of Ln^{+3} and Ta^{+5}, the lithium content was constrained to five Li^+ per formula unit. This was done by manually adjusting the occupancies of the Td and Oh sites to the values obtained from a neutron study of $La_3Li_5Ta_2O_{12}$. [22] This assumes that no oxygen vacancies or OH^- groups partially substituting for O^{2-} anions are present. Refinement of the oxygen site occupation factor gave a value greater than unity, and it was therefore fixed at 1.00. The Li occupancies were thus set at: Td site 80.7% occupied; Oh site 43% occupied. The refined lithium U_{iso} values derived from this are still 3–4 times larger than those of the metal and oxygen atoms. This likely reflects the positional disorder observed in the neutron study, i.e. the reported lithium positions are averages of more than one independent position. The largest peaks and holes remaining in the final difference maps of this model are: Ln = La: +2.3 and −1.8 e$^-$/Å^3, both located < 0.6 Å from Ta_1; Ln = Pr: +1.8 and −1.6 e$^-$/Å^3, located 0.57 Å from Ta_1 and 0.67 Å from Li_1, respectively, and Ln = Nd: +2.3 and −1.8 e$^-$/Å^3, both located < 0.6 Å from Ta_1. It must be noted that, although the present X-ray refinement clearly shows the presence of lithium in both tetrahedral and octahedral sites, the precise amount and location of Li in both sites of course

Table 2
Atomic coordinates and equivalent isotropic displacement parameters (Å$^2 \times 10^3$) for $La_3Li_5Ta_2O_{12}$, $Pr_3Li_5Ta_2O_{12}$ and $Nd_3Li_5Ta_2O_{12}$.

	x	y	z	U_{eq}
$La_3Li_5Ta_2O_{12}$				
La_1	0.1250	0	0.2500	0.009(1)
Ta_1	0	0	0	0.006(1)
O_1	0.2795(3)	0.1050(3)	0.1989(3)	0.008(1)
Li_1	0.3750	0	0.2500	0.034(8)
Li_2	0.1250	0.683(3)	0.567(3)	0.034(80
$Pr_3Li_5Ta_2O_{12}$				
Pr_1	0.1250	0	0.2500	0.007(1)
Ta_1	0	0	0	0.008(1)
O_1	0.2790(2)	0.1041(2)	0.1967(2)	0.007(1)
Li_1	0.3750	0	0.2500	0.028(6)
Li_2	0.1250	0.684(3)	0.566(3)	0.035
$Nd_3Li_5Ta_2O_{12}$				
Nd_1	0.1250	0	0.2500	0.008(1)
Ta_1	0	0	0	0.006(1)
O_1	0.2790(2)	0.1034(2)	0.1973(2)	0.008(1)
Li_1	0.3750	0	0.2500	0.026(6)
Li_2	0.1250	0.686(3)	0.564(3)	0.044(11)

U(eq) is defined as one third of the trace of the orthogonalized U^{ij} tensor.

Table 3
Selected interatomic distances (Å) for $La_3Li_5Ta_2O_{12}$, $Pr_3Li_5Ta_2O_{12}$ and $Nd_3Li_5Ta_2O_{12}$.

	$La_3Li_5Ta_2O_{12}$	$Pr_3Li_5Ta_2O_{12}$	$Nd_3Li_5Ta_2O_{12}$
Ln(1)–O(1) (× 4)	2.474(4)	2.447(3)	2.429(3)
Ln(1)–O(1) (× 4)	2.581(3)	2.529(3)	2.527(3)
Ta–O(1) (× 6)	1.999(3)	2.000(3)	1.996(3)
Li(1)–O(1) (× 4)	1.928(4)	1.914(3)	1.898(3)
Li(2)–O(1) (× 2)	2.351(3)	2.354(3)	2.335(3)
Li(2)–O(1) (× 2)	2.44(4)	2.38(4)	2.34(5)
Li(2)–O(1) (× 2)	1.99(4)	1.99(3)	2.00(4)

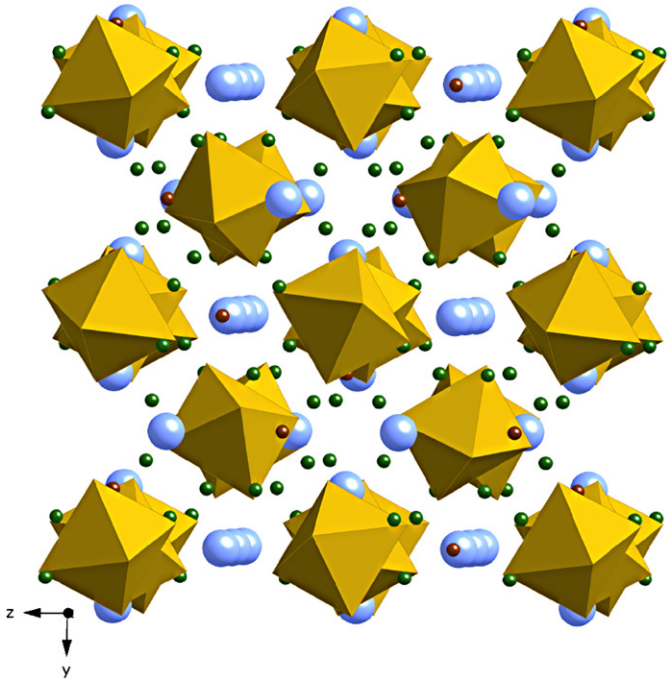

Fig. 2. Schematic of the crystal structure of $Ln_3Li_5Ta_2O_{12}$. TaO_6 polyhedra are shown in yellow and Ln^{3+} are shown as light blue spheres. Octahedrally and tetrahedrally coordinated Li^+ ions are shown in green and brown, respectively. Oxygen atoms are omitted for clarity.

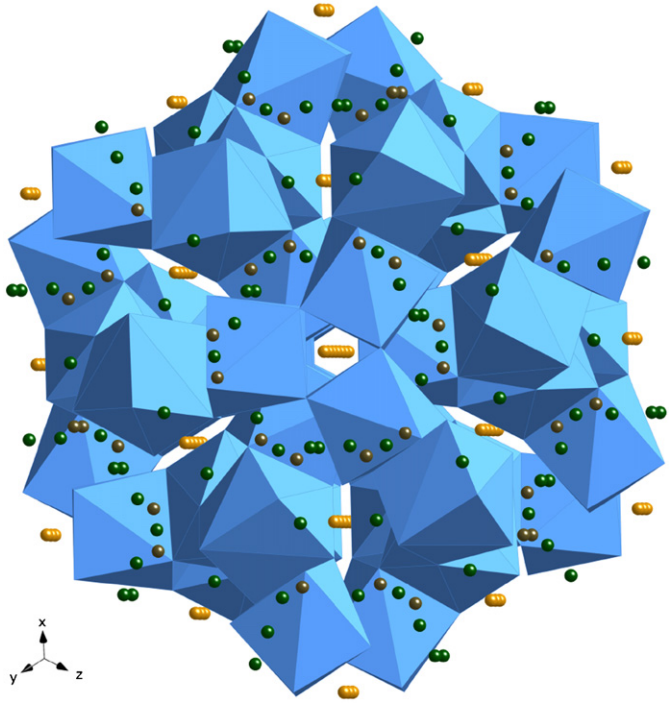

Fig. 3. An alternative view of the structure of $Ln_3Li_5Ta_2O_{12}$ viewed along the [111] direction. LnO_8 polyhedra are shown in blue. Ta^{5+} atoms are shown as yellow spheres. Octahedrally and tetrahedrally coordinated Li^+ atoms are in green and brown, respectively. Oxygen atoms are omitted for clarity.

cannot be established with certainty. Relevant crystallographic data for $Ln_3Li_5Ta_2O_{12}$ (Ln = La, Pr, Nd) are listed in Table 1. For all three compounds, atomic positions are listed in Table 2 and selected interatomic distances and bond angles are compiled in Table 3.

2.4. UV–visible spectrometry

The diffuse-reflectance spectrum of ground crystals of $Nd_3Li_5Ta_2O_{12}$ was collected using a Perkin-Elmer Lambda 35 UV/Vis Scanning Spectrophotometer equipped with an integrating sphere. Due to the previous report of $La_3Li_5Ta_2O_{12}$ and the extremely low yield of $Pr_3Li_5Ta_2O_{12}$ the UV–Vis spectra for those compounds were not recorded and will not be discussed in this paper.

2.5. Impedance spectroscopy

The transport properties of $Nd_3Li_5Ta_2O_{12}$ were evaluated using a Solartron 1260 impedance analyzer. A pellet with a diameter of 12 mm and thickness of 5 mm was prepared by sintering at 600 °C for 48 h. Platinum electrodes were attached to the opposing faces of a sintered pellet using a platinum paste. After drying under ambient conditions this assembly was heated to 500 °C in air in order to cure the contacts before any impedance data were collected. Data were collected in air in the temperature range $300 \leqslant T(^\circ C) \leqslant 500$ using a driving voltage of 0.1 V over a frequency range of 1 Hz to 10 MHz and analyzed using the ZVIEW3.0 software. Data were collected after the 2 h of isothermal treatment.

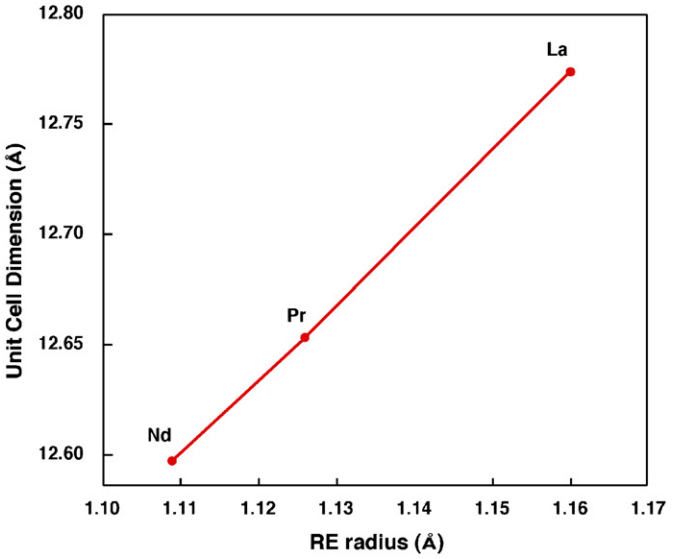

Fig. 4. Plot of the unit cell parameter a versus the ionic radius of the lanthanide ion present in the $Ln_3Li_5Ta_2O_{12}$ structure.

3. Results and discussion

3.1. Crystal structure

Single crystals of $Ln_3Li_5Ta_2O_{12}$ (Ln = La, Pr, Nd) were grown out of a reactive lithium hydroxide melt and found to crystallize in the cubic space group $Ia\bar{3}d$ (No. 230) with lattice parameters of $a = 12.7735(1)$, 12.6527(1), and 12.5967(1) Å for $La_3Li_5Ta_2O_{12}$, $Pr_3Li_5Ta_2O_{12}$, and $Nd_3Li_5Ta_2O_{12}$, respectively. The three oxides are part of a larger family of garnet related oxides with general formula $Ln_3Li_5M_2O_{12}$ (Ln = La, M = Nb, Ta, Sb) [8,31,32]. The structures have been discussed extensively, with special emphasis on the difficulty of locating of the lithium atoms within the matrix [8,22,24,30,31,33]. The refinement of light atoms, such as lithium, in the presence of heavy atoms such as Ln and Ta, is known to be difficult and thus we first refined the non-lithium atomic positions Ln_1, Ta_1 and O_1. Refinement of this model converged rapidly in all cases. Refinement of the remaining main peaks in the difference map, corresponding to tetrahedral and octahedral sites, as fully occupied lithium atoms yielded unreasonable thermal parameters and an excess of positive charge. However, the site occupancy refinements for lithium atoms showed a decrease from unity and yielded more stable refinements. However, this occupancy refinement resulted in only three lithium atoms per formula unit, thus, leading to an excess charge of −2 per formula unit, while charge neutrality requires the presence of five Li^+ atoms. As it was not possible to identify additional lithium sites and achieve a stable refinement, we fixed the lithium ion occupancy using the data for $La_3Li_5Ta_2O_{12}$ from the neutron study by Cussen, [22] which is expected to be more sensitive to the lithium ions. Using these fixed lithium positions, the refinements of all three structures were completed. Clearly there are lithium atoms in both tetrahedral and octahedral sites, however, due to the limitations of the technique, the exact positions and occupancies of the lithium ions cannot be positively established by X-ray diffraction methods.

The structure of $Ln_3Li_5Ta_2O_{12}$ consists of the $[Ln_3Ta_2O_{12}]^{5-}$ network of isolated TaO_6 octahedra edge-shared to the LnO_8

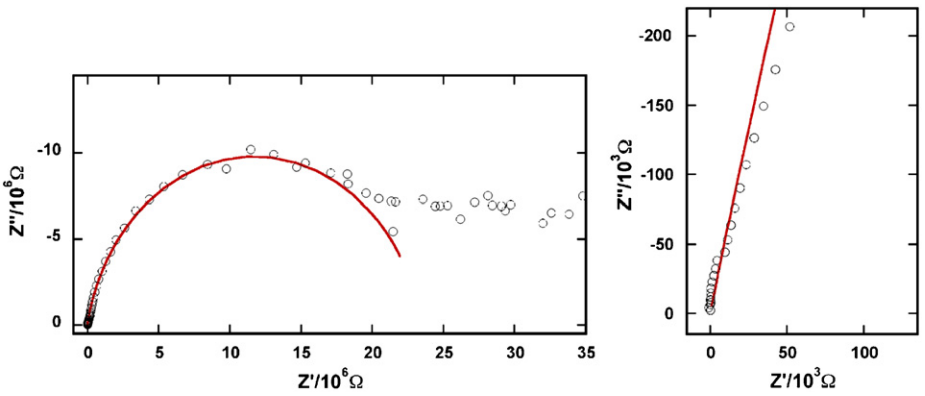

Fig. 5. (a) A Cole–Cole plot of the impedance data collected at 300 °C. The solid line shows a fit based on an equivalent circuit consisting of a parallel arrangement of a constant phase element and resistor. (b) High frequency portion of the plot of the impedance spectrum.

cubes, which form an infinite chain within the structure. These coordination environments are typical for Ln^{3+} and Ta^{5+} ions. Fig. 2 depicts this interconnected network of the TaO_6 octahedra with isolated Ln^{3+} atoms located in the cavities of the network. Fig. 3 shows the alternative view along [111] plane that reveals the interconnected matrix of LnO_8 units. This network contains the cavities occupied by Ta^{5+} cations. Two different kinds of lithium atoms are disordered in a complex fashion among the tetrahedral and octahedral sites, where the distribution of the Li^+ atoms over the *Oh* and *Td* sites allows for a three dimensional conduction pathway. The substitution of the smaller lanthanides, Pr and Nd, for La, causes an expected decrease in the unit cell parameter *a*, which is graphically depicted in Fig. 4.

3.2. Li^+ conductivity in $Nd_3Li_5Ta_2O_{12}$

Impedance measurements on $Nd_3Li_5Ta_2O_{12}$ were unable to detect any ion mobility at room temperature. On heating the sample to 300 °C the conductivity increased to a measurable level of $\sigma_{300\,^\circ C} \approx 10^{-8}\,S\,cm^{-1}$. However, it was not possible to resolve inter- and intra-grain contributions to the impedance and so values for conductivity were extracted by modeling the high frequency portion of the data with an equivalent circuit containing a parallel arrangement of a constant phase element and resistor to give the fit shown in Fig. 5(a) and (b). This limited analytical approach is broadly comparable to that employed in the literature [9] and yields values of conductivity that are between six and nine orders of magnitude smaller than reported in other lithium-stuffed garnets such as $Li_{3+x}Nd_3Te_{2-x}Sb_xO_{12}$ [34] and $Li_7BaLa_2Zr_2O_{12}$ [12]. Reports of the transport properties of the La-analog, $Li_5La_3Ta_2O_{12}$, have indicated that this compound shows a Li conductivity of $10^{-2}\,S\,cm^{-1}$ at 300 °C [9]. Data collected up to 475 °C could be analyzed in the same way to give the values for conductivity shown in Fig. 6.

Data collected at 500 °C showed that the conductivity varied by an order of magnitude as a function of thermal history, suggesting that the microstructure was changing at this temperature and changing the intergrain Li^+ conductivity. This variability and the extremely high values of impedance make it difficult to extract quantitative information from these data. However, it is clear that the transport of lithium through this material differs spectacularly from that in related phases; our data show that the bulk conductivity of $Li_5Nd_3Ta_2O_{12}$ is six orders of magnitude smaller than $Li_5La_3Ta_2O_{12}$. Previous reports have concluded that the microstructure can cause a variation of up to one order of magnitude in the total conductivity [9]. These data show that either: (i) the lithium ions are immobile in the $Li_5Nd_3Ta_2O_{12}$ lattice or (ii) the microstructure of this material blocks the passage of lithium ions through the bulk of the material in a way that has not been observed in any of the garnets studied to date. The similarities between the crystal structure of $Li_5Nd_3Ta_2O_{12}$ and fast-ion conducting garnets suggests that unusual microstructural effects are responsible for the poor total conductivity of Li^+ in this compound.

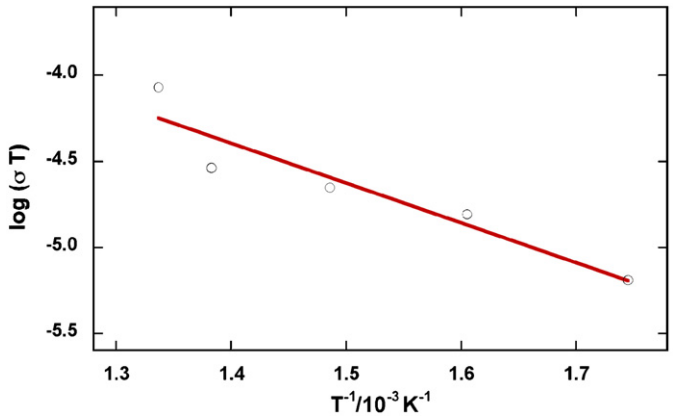

Fig. 6. An Arrhenius plot for the conductivity data collected in the temperature range of 300–475 °C.

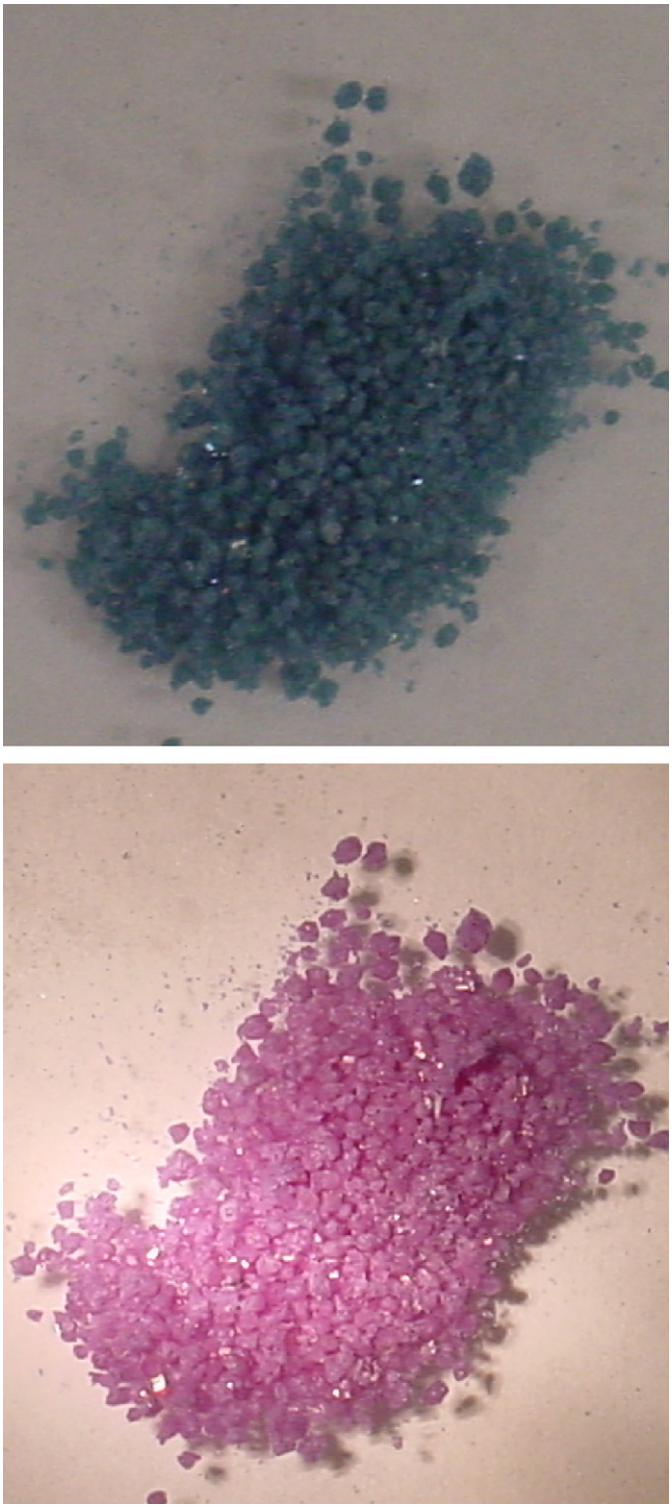

Fig. 7. Optical images of $Nd_3LI_5Ta_2O_{12}$ crystals illuminated by: (a) a standard fluorescent light bulb and (b) a standard incandescent light bulb.

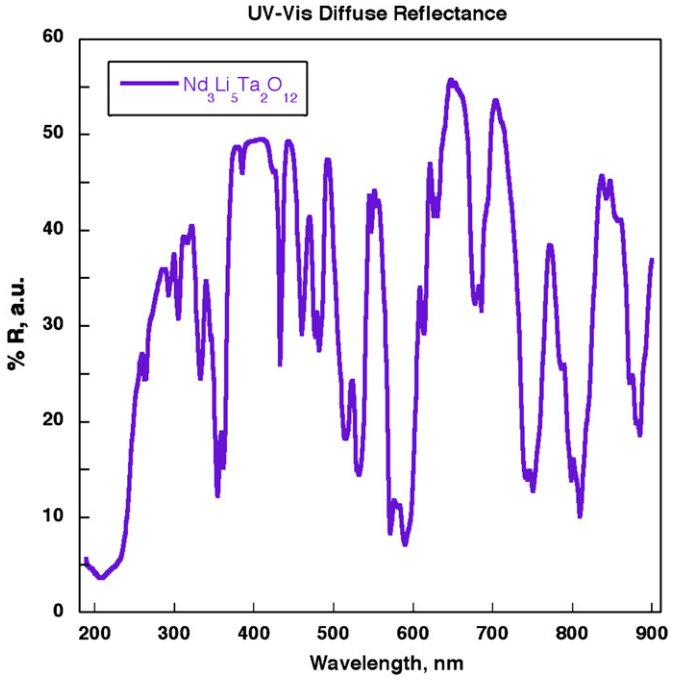

Fig. 8. UV–Vis diffuse reflectance spectrum of $Nd_3Li_5Ta_2O_{12}$.

3.3. *Alexandrite effect in* $Nd_3Li_5Ta_2O_{12}$

We observed that $Nd_3Li_5Ta_2O_{12}$ changes color as a function of the light source used for illumination. Specifically, the oxide appears purple in sunlight or when using a regular incandescent light bulb, while it appears blue under a standard fluorescent light bulb. This color change is depicted in Fig. 7, which shows optical images of crystals of $Nd_3Li_5Ta_2O_{12}$ under: (a) incandescent light and (b) fluorescent light. This type of dichroism is found in the naturally occurring mineral alexandrite [26] and as a result, materials that change color in this fashion are described as exhibiting an "alexandrite effect". There have been reports of naturally occurring Nd^{3+} containing minerals exhibiting this effect [27], which in the case of Nd is generally attributed to the sharp peaks in the visible portion of the reflectance spectrum. To explain the color change of $Nd_3Li_5Ta_2O_{12}$, we collected the UV–Vis diffuse reflectance spectrum shown in Fig. 8. Since there exist distinct narrow bands in the visible part of the spectrum around 440, 460, 480, 525, 580, 620 and 660 nm, even a slight difference in the spectral composition of the incident light source will result in a change of absorbance and, consequently, a color change of the oxide. This phenomenon is in fact observed in many Nd containing oxides, including Nd_2O_3.

4. Conclusions

We have reported the flux synthesis of single crystals of a series of lanthanide-containing tantalates, $Ln_3Li_5Ta_2O_{12}$ (Ln = La, Pr, Nd) and discussed their crystal structures. These lithium-rich garnets are of general interest for the lithium ion conductivity due to the partial occupancy of the lithium sites in the structure, however, the study reported in this paper exhibits a surprisingly low bulk cation conductivity. $Nd_3Li_5Ta_2O_{12}$ was examined for its unusual dichroism (alexandrite effect) and its UV–Vis diffuse reflectance spectrum was used to explain this optical phenomenon.

Supplementary data

Further details of the crystal structure investigation can be obtained from the Fachinformationszentrum Karlsruhe, 76344 Eggestein-Leopoldshafen, Germany (fax: +497247808666; e-mail: crystaldata@fiz-karlsruhe.de) on quoting the depository numbers CSD—419624 for $La_3Li_5Ta_2O_{12}$ CSD—419625 for $Nd_3Li_5Ta_2O_{12}$ and CSD—419626 for $Pr_3Li_5Ta_2O_{12}$.

Acknowledgments

This work was supported by the National Science Foundation through Grants DMR:0450103 and DMR:0804209. We would like to thank Prof. Mudring for making us aware of the Alexandrite effect.

References

[1] W.R. Gemmill, M.D. Smith, H.-C. zur Loye, J. Solid State Chem. 177 (2004) 3560.
[2] S.J. Mugavero III, M.D. Smith, H.-C. zur Loye, J. Solid State Chem. 178 (2005) 200.
[3] W.R. Gemmill, M.D. Smith, H.-C. zur Loye, J. Solid State Chem. 179 (2006) 1750.
[4] S.J. Mugavero III, M.D. Smith, H.-C. zur Loye, Solid State Sci. 9 (2007) 555.
[5] M. Bharathy, V.A. Rassolov, H.-C. zur Loye, Chem. Mater. 20 (2008).
[6] I.P. Roof, S. Park, T. Vogt, V.A. Rassolov, M.D. Smith, S. Omar, J. Nino, H.-C. zur Loye, Chem. Mater. 20 (2008) 3327.
[7] I.P. Roof, M.D. Smith, H.-C. zur Loye, J. Cryst. Growth 310 (2008) 240.
[8] D. Mazza, Mater. Lett. 7 (1988) 205.
[9] V. Thangadurai, H. Kaak, W. Weppner, J. Am. Ceram. Soc. 86 (2003) 437.
[10] J. Percival, P.R. Slater, Solid State Comm. 142 (2007) 355.
[11] R. Murugan, W. Weppner, P. Schmid-Beurmann, V. Thangadurai, Mater. Sci. Eng. B 143 (2007) 14.
[12] R. Murugan, V. Thangadurai, W. Weppner, Angew. Chem. Int. Ed. 46 (2007) 7778.
[13] E. Kendrick, J. Kendrick, K.S. Knight, M.S. Islam, P.R. Slater, Nat. Mater. 6 (2007) 871.
[14] V. Thangadurai, W. Weppner, J. Solid State Chem. 179 (2006) 974.
[15] Q.N. Pham, C. Bohnke, J. Emery, O. Bohnke, F. Le Berre, M.-P. Crosnier-Lopez, J.-L. Fourquet, P. Floirian, Solid State Ionics 176 (2005) 495.
[16] V. Lupei, A. Lupei, A. Ikesue, Opt. Mater. 30 (2008) 1781.
[17] J. Sulc, H. Jelinkova, T.T. Basiev, M.E. Doroschenko, L.I. Ivleva, V.V. Osiko, P.G. Zverev, Opt. Mater. 30 (2007) 195.
[18] L. Chaiyapoom, S. Wongnawa, C. Pakawatchai, J. Charmant, S. Saithong, Inorg. Chem. Comm. 9 (2006) 316.
[19] E. Cavalli, A. Belletti, S. Bigotta, A. Toncelli, M. Tonelli, J. Alloys Compd. 365 (2004) 1.
[20] M.P. O'Callaghan, E.J. Cussen, Solid State Sci. 10 (2008) 390.
[21] E. Kendrick, M.S. Islam, P.R. Slater, J. Mater. Chem. 17 (2007) 3104.
[22] E.J. Cussen, Chem. Commun. (2006) 412.
[23] H.M. Kasper, Inorg. Chem. 8 (1969) 1000.
[24] M.P. O'Callaghan, A.S. Powell, J.J. Titman, G.Z. Chem, E.J. Cussen, Chem. Mater. 20 (2008) 2360.
[25] Z. Hu, Z. Lin, G. Wang, J. Solid State Sci. 177 (2004) 3028.
[26] G. Steffen, Farbe und Lumineszenz von Mineralien: Einfuhrung in die kristallchemischen und kristallphysilaischen Ursachen, Enke im Georg-Thieme-Verl, 2000.
[27] L.R. Bernstein, Am. Min. 67 (1982) 356.
[28] SMART Version 5.630, SAINT+Version 6.45, SADABS Version 2.10 Bruker Analytical X-ray Systems, Inc., Madison, 2003.
[29] G.M. Sheldrick, SHELXTL, Bruker Analytical Systems, Inc, Madison, 2000.
[30] V. Thangadurai, S. Adams, W. Weppner, Chem. Mater. 16 (2004) 2998.
[31] H. Hyooma, K. Hayashi, Mater. Res. Bull. 23 (1988) 1399.
[32] J. Isasi, M.L. Veiga, R. Saez-Puche, A. Jerez, C. Pico, J. Alloys Compd. 177 (1991) 251.
[33] E.J. Cussen, T.W.S. Yip, J. Solid State Chem. 180 (2007) 1832.
[34] M.P. O'Callaghan, E.J. Cussen, Solid State Sci. 10 (2008) 390.